POLİTEKNİK DERGİSİ

JOURNAL of POLYTECHNIC

ISSN: 1302-0900 (PRINT), ISSN: 2147-9429 (ONLINE)

URL: http://dergipark.org.tr/politeknik

Curve/probabilistic fitting of damage metrics for Al-7075 materials behavior by using electromechanical impedance method

Elektromekanik empedans yöntemi kullanılarak Al-7075 malzeme davranışı için hasar metriklerinin eğrisel/olasılıksal tahmini

***Yazar(lar) (Author(s))**: Gökhan HAYDARLAR[1], Mesut TEKKALMAZ[2], M. Alper SOFUOĞLU[3]*

ORCID[1]: 0000-0001-7430-8145

ORCID[2]: 0000-0003-3781-0384

ORCID[3]: 0000-0003-4681-6390

Bu makaleye şu şekilde atıfta bulunabilirsiniz(To cite to this article): Haydarlar G., Tekkalmaz M. ve Sofuoğlu M. A., "Curve /probabilistic fitting of damage metrics for Al-7075 materials behavior by using electromechanical impedance method", ***Politeknik Dergisi***, 24(2): 481-494, (2021).

Erişim linki (To link to this article): http://dergipark.org.tr/politeknik/archive

DOI: **10.2339/politeknik.698644**

Curve/Probabilistic Fitting of Damage Metrics for Al-7075 Materials Behavior by Using Electromechanical Impedance Method

Highlights

- *The behavior of constrained piezoelectric wafer active sensor (PWAS)/Al-7075 was investigated.*
- *It is aimed to compensate for the temperature effect using EFS and curve/probabilistic fitting.*

Graphical Abstract

The behavior of the constrained piezoelectric sensor/Al-7075 has been investigated at varying temperatures.

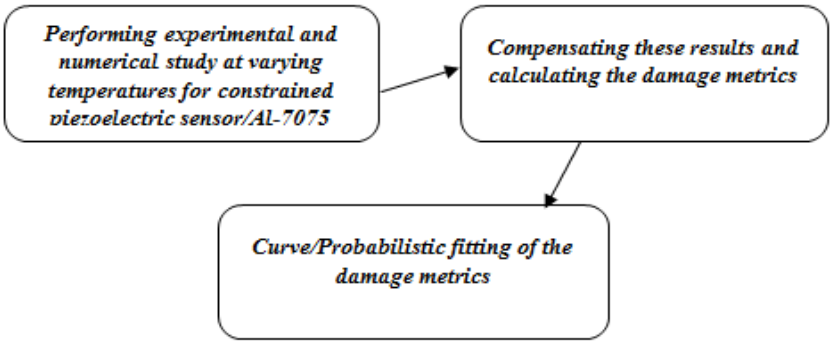

Figure 1. Flowchart of the study

Aim

This study aims to observe the behavior of the constrained piezoelectric sensor/Al-7075 at varying temperatures using the experimental and finite element method. In addition, it is aimed to compensate for the temperature effect after the experimental and numerical results are obtained.

Design & Methodology

In this study, the behavior of the constrained piezoelectric sensor/Al-7075 was studied at varying temperatures by using the experimental and finite element method. After experimental and numerical studies, it is aimed to compensate for the temperature effect using a compensation algorithm and curve/probabilistic fitting.

Originality

The numerical studies for the behavior of the constrained piezoelectric sensor/Al-7075 at varying temperatures are limited in the literature. All the experimental and numerical results are compensated for the temperature effect and analyzed using curve/probabilistic fitting for the first time.

Findings

It has been observed that as the temperature decreases, the frequency shifts to the right (increases) and the amplitude increases. This change has been compensated by using EFS. Three damage metrics decreased significantly after compensation. The best curves for RMSD, MAPD and CCDM were Richards, Exponential Association 3, and Sinusoidal curves, respectively, for non-compensated results. Johnson SB distribution for RMSD, MAPD and Error distribution for CCDM were the most appropriate distributions for experimental compensated damage metrics. Experimental and simulation results are close to each other.

Conclusion

In this study, Al-7075 sample was chosen for the experimental research, considering these structures exposed to varying ambient temperatures. A finite element model considering the temperature effect on the piezoelectric sensor and Al-7075 sample was proposed. The behavior of the constrained piezoelectric sensor/Al-7075 for varying temperatures has been investigated. EMI technique has great potential, much work is being done to resolve several problems. Future studies should focus more on real structures to identify critical problems using the EMI technique because most of the researches are conducted under laboratory conditions.

Declaration of Ethical Standards

The authors of this article declare that the materials and methods used in this study do not require ethical committee permission and/or legal-special permission.

Curve/Probabilistic Fitting of Damage Metrics for Al-7075 Materials Behavior by Using Electromechanical Impedance Method

Araştırma Makalesi / Research Article

Gökhan HAYDARLAR, Mesut TEKKALMAZ, M. Alper SOFUOĞLU*

Eskişehir Osmangazi University, Mechanical Engineering Department, 26040, Eskişehir, Turkey

(Geliş/Received : 04.03.2020 ; Kabul/Accepted : 10.04.2020)

ABSTRACT

The purpose of structural health monitoring is to provide information by making a simultaneous diagnosis of the status of the structure. Despite aging, environmental conditions and unforeseen circumstances, the construction should remain as specified in the design. Changing the environmental conditions causes the sensor and the host structure to change material properties. It is essential to take into account environmental conditions to prevent misdiagnosis. Therefore, the real cause of the change can be determined.

In this study, the behavior of constrained piezoelectric wafer active sensor (PWAS)/Al 7075 was investigated by using electromechanical impedance method (EMI) under changing environmental conditions. Numerical studies on this material in the literature are limited and all the experimental/ numerical results are compensated for the temperature effect and analyzed using curve/probabilistic fitting approach for the first time. The sample used in the experimental work was modeled in ANSYS finite element program. In the experimental and numerical results, it has been observed that as the temperature decreases, the frequency shifts to the right and the amplitude increases. The experimental and simulation results were nearly the same. The temperature effect was compensated using the compensation algorithm for experimental and numerical studies. The results were compared using damage metrics. The experimental results were analyzed using a curve/probabilistic fitting approach.

Keywords: Structural health monitoring, piezoelectric sensors, electromechanical impedance method, temperature effect, damage metrics, curve fitting.

Elektromekanik Empedans Yöntemi Kullanılarak Al-7075 Malzeme Davranışı İçin Hasar Metriklerinin Eğrisel / Olasılıksal Tahmini

ÖZ

Yapısal sağlık izlemenin amacı, yapının durumunun eş zamanlı teşhisini yaparak bilgi sağlamaktır. Yaşlanmaya, çevresel koşullara ve öngörülemeyen koşullara rağmen yapı tasarımda belirtildiği gibi kalmalıdır. Çevresel koşulların değiştirilmesi, sensör ve eklendiği yapının malzeme özelliklerini değiştirmesine neden olur. Yanlış teşhisi önlemek için çevresel koşulları dikkate almak önemlidir. Bu sayede, değişimin gerçek nedeni belirlenebilir.

Bu çalışmada değişen çevresel koşullar altında sınırlandırılmış piezoelektrik sensörün (PWAS)/Al davranışı elektromekanik empedans (EMI) yöntemi kullanılarak araştırılmıştır. Literatürde bu materyal üzerinde yapılan sayısal çalışmalar sınırlıdır. Tüm deneysel / sayısal sonuçlar sıcaklık etkisi için telafi edilmiştir ve ilk kez eğri/olasılıksal tahmin yaklaşımı kullanılarak analiz edilmiştir. Deneysel çalışmada kullanılan numune ANSYS sonlu elemanlar programında modellenmiştir. Deneysel ve sayısal sonuçlarda sıcaklık azaldıkça frekansın sağa doğru kaydığı ve genliğin arttığı gözlenmiştir. Deneysel ve sayısal sonuçların yakın olduğu belirlenmiştir. Sıcaklık etkisi, deneysel ve sayısal çalışmalar için telafi algoritması kullanılarak telafi edilmiştir. Sonuçlar hasar metrikleri kullanılarak karşılaştırılmıştır. Deneysel sonuçlar bir eğri/olasılıksal tahmin yaklaşımı kullanılarak analiz edilmiştir.

Anahtar Kelimeler: Yapısal sağlık izleme, piezolektrik sensörler, elektromekanik empedans yöntemi, sıcaklık etkisi, hasar metrikleri, eğri uydurma.

1. INTRODUCTION

Due to loading and environmental influences, there is constant deterioration in strength after the construction of mechanical, space and aviation structures. At the time of construction, it is impossible to provide consistent quality and strength for these structures. Therefore, there are differences in strength between structures. The difference can be considered to be undamaged if the threshold is below a specific value. Due to specific reasons, such as overload, changing environmental conditions, or fatigue, the difference may cause the damage to occur above the threshold limit if it increases. If the difference rises above the threshold value, the component cannot fulfill its task within the structure. Damage and failure are interrelated terms and vary from structure to structure. For example,

*Sorumlu Yazar (Corresponding Author)
e-posta: asofuoglu@ogu.edu.tr

the failure threshold limit in aviation structures is much lower than in buildings [1].

Structural health monitoring (SHM) is a process in which specific strategies are applied to determine the damage's location/size and the remaining life of the structure after the damage has occurred. With SHM, the response of the structural system or components under different loading and environmental conditions is continuously measured. SHM is used to monitor and assess the status and abnormalities of structures and components in the working situation during and after unexpected situations, due to damage [2].

SHM includes observing the dynamic response of the system with the help of sensors at regular intervals and determining the current state of operation using statistical analyzes. In the long run, this process is regularly updated to provide information on whether or not the output of the process is performing its predetermined functions. After non-deterministic events such as earthquakes, SHM is used for rapid status scanning and aims to provide reliable information on the integrity of the structure in real-time [3].

A successful SHM design requires the recognition and integration of the various components. The definition of health and performance metrics is the first component that needs basic knowledge. Unexpected situations can be encountered in buildings and structures. These situations emphasize the importance of automated health monitoring systems. These automated systems provide improving the performance of the buildings and structures with an excellent benefit/cost ratio and long-term benefits [1]

There are many studies within the scope of piezoelectric material characterization in structural monitoring in the literature. Hooker [4] experimentally investigated the temperature changes of the piezoelectric charge constants (d_{31} and d_{33}) of piezoelectric ceramics PZT 4, PZT 5A, PZT 5H between -150 °C and 250 °C and relative thermal expansion between 25 °C and 600 °C. All of the materials assessed in this study have suitable properties for use in aviation applications. They concluded that it is more important to consider when selecting materials for the applications where low temperature (i.e., < -50 °C) or high temperature (i.e., > 150 °C) characteristics that various properties of the material considerably deviate from room temperature behavior. Grisso and Inman [5] investigated the slope of the susceptance at varying temperatures. Sepehry et al. [6] presented a theoretical model considering piezoelectric wafer active sensor (PWAS) and Al 2024 material properties at different temperatures to determine the behavior of Al 2024 with PWAS at different temperatures. Experiments were carried out at 25 °C to 50 °C temperature range to validate the model. They indicated that theoretical and experimental studies are compatible. As a result of experimental and theoretical studies, it has been obtained that the real part of the impedance decreases because the increasing temperature changes the material properties of PWAS and it has been observed that natural frequency shifts horizontally to the left due to the change of the aluminum material properties with increasing temperature. Freitas et al. [7] found piezoelectric, mechanical and elastic properties of (0.6) $BiFeO_3$- (0.4) $PbTiO_3$ ceramics focusing on high-temperature applications. Piezoelectric coefficients, g_{31} (piezoelectric voltage constant) and d_{31} (piezoelectric charge constant) are as high as other commercial piezo ceramics at room temperature with increasing temperature; these coefficients are stable at temperature (20 °C - 100 °C and 250 °C - 300 °C). They have concluded that the piezoelectric constants can be used as transducers and actuators for high-temperature applications due to their thermal stability at high temperatures. Gupta et al. [8] developed and experimentally validated a new draft for active structural vibration control using PZT 5H patches at high temperatures. The control law is derived by taking into account the variation of the piezoelectric stress coefficient (ε_{11}) and the dielectric constant (ε_{33}) with temperature in the piezoelectric equations. Since the dependence of ε_{11} and ε_{33} parameters on the temperature is analytically unknown, they have determined the temperature change of these parameters by curve fitting using experimentally measured data at high temperatures. Experiments have been carried out in cases where the variation of the ε_{11} and ε_{33} parameters for the active vibration control plate between 25 °C and 75 °C is considered and neglected. The active vibration control has concluded that ε_{11} and ε_{33} parameters can be sustained at high temperatures when the temperature change is taken into consideration, while their performance cannot be sustained if they are neglected. Bukhari et al. [9] determined the temperature change of the piezoelectric charge constant d_{15} at cryogenic temperatures (between 0 K and 300 K) for different ceramics (PZT, $LiNbO_3$, and PMN-PT). This change is almost linear for PZT, $LiNbO_3$ has the smallest $d_{15,}$ and PMN-PT has the largest d_{15} value at room temperature. They determined that the d_{15} values for $LiNbO_3$ and PMN-PT at the lowest temperatures are about 6% and 8%, respectively. Applications such as accurate stress measurement and calibration depend on the d_{15} parameter and temperature. As a result of this study, it was stated that the change in temperature was nearly the same, in $LiNbO_3$ and other ceramics, the change was particularly great at low temperatures. Baptista et al. [10] studied the effect of temperature on electromechanical impedance signals in SHM. Zou et al. [11] investigated the amplitude of the signals detected at varying temperatures (30 °C, 40 °C, 50 °C, 60 °C, 70 °C, 80 °C) by introducing harmonic signals at different frequencies

(1-10-100-1000 Hz). Artificial neural network algorithms and optimization algorithms are widely common in structural health monitoring applications [12-13]. Rabelo et al. [14] offered a statistical model for damage detection at varying temperatures (-10 °C to 60 °C) on Al 2024-T3 plates. Wandowski et al. [15] investigated the effect of temperature change on the real part of impedance (resistance) for damaged and undamaged states of carbon fiber reinforced polymers. Xu et al.[16] proposed a spectral element method to predict admittance by considering the effect of temperature on the piezoelectric sensor and structure attached to the surface. Haider et al. [17] found the material properties of the circular piezoelectric sensor at varying temperatures (50 °C - 250 °C). Rezvani et al. [18] compared four different methods to identify the damages in the structures. A steel beam with constant rectangular cross-section was used to compare these methods. It was obtained that the proposed methods can detect the damages easily. In terms of FEM modeling, there are several studies in the literature. Tseng and Wang [19] performed both experimental and numerical studies to two concrete beam structures, which resulted in increased root mean square deviation (RMSD) values when crack damage increased and closer to PZT transducers. Yang et al.[20] used ANSYS to apply the Electromechanical Impedance (EMI) technique to several models, including joining layers on an aluminum beam, and it was found that a perfect fit compared to experimental data up to 1000 kHz. The authors also simulated the EMI technique in the frequency range from 30-60 °C to 400 kHz and simulation results fit well with experimental results. Lim and Soh [21] studied the use of EMI technique to estimate the remaining fatigue life of the aluminum structure via ANSYS 12.1. While characterizing crack lengths during their studies, they stated that correlation coefficient deviation metric (CCDM) results showed better results than RMSD. Hamzeloo et al. [22] studied the EMI method to perform both experiments and simulations using ABAQUS on aluminum and steel samples. The test samples were hollow cylinders of different thicknesses, and the test was carried out in the frequency range of 10 to 40 kHz. Via RMSD metric, the results showed that the increase in damage does not always increase the RMSD values.

By using appropriate SHM methods, situations that cannot be detected in the early stages is appropriately determined, thus contributing to the development of countries' economies. Appropriate precautions can be taken if damage or cracks are detected early in the process before the building is unable to function. The collapse of bridges, tall buildings and other essential structures, accidents caused by train tracks, and accidents that occur in air crafts prevent the economic growth of the country and cause human resources to be lost at the same time. Constructions are designed for a specific lifetime, and it is assumed that during this time, the build is functioning correctly. With the help of appropriate SHM methods, it is possible to make considerable savings by increasing the lifetime of the structure and increasing its maintainability [1].

In this study, the behavior of the constrained piezoelectric sensor/Al 7075 at varying temperatures was studied by using the experimental and finite element method considering the effect of environmental conditions. The reason for selecting aluminum is that Al 7075 is widely used in aviation applications and exposed to varying ambient temperatures during operation. After experimental and numerical studies, it is aimed to compensate for the temperature effect by using a compensation algorithm. Numerical studies on this material in the literature are limited and this is the motivation of the study. Also, all the experimental and numerical results are compensated for the temperature effect and analyzed using curve/probabilistic fitting for the first time. This work will contribute to damage control of the aviation structures in the industry. The study includes five parts. In the second section, experimental and numerical methods are given. Then, experimental/numerical results are explained, and temperature compensation is presented. After that, the experimental results are analyzed using curve/probabilistic fitting. In the end, the conclusion section is given.

2. EXPERIMENTAL and NUMERICAL METHOD

2.1. Experimental Method

Al 7075 sample was used in the experimental study. The sample used in the experiments is given in Fig.1. The dimensions of the sample were 30x30x3 mm. In the next step, impedance measurements of the samples were performed, at room temperature using Keysight E4990A impedance analyzer. Impedance measurements of the samples at varying temperatures were performed using the ARTICO LFE140 laboratory cooler (Fig.2). Experimental measurements were carried out with a temperature from -10 °C to -45 °C at 5 °C intervals.

Figure 1. Al-7075 sample

Figure 2. Cooler

Aluminum is widely used in aircraft parts, space and defense industry applications. In aviation applications, aircraft are subjected to varying ambient temperatures ranging from -55 °C to 80 °C [14]. Generally, aircraft body parts are lower than 0°C, so -10 °C to -45 °C temperature interval is taken into consideration in this study.

A 10x10x0.5 mm piezoelectric sensor was bonded to the Al 7075 using M-Bond 200 adhesive. Then one of the probes was attached to the piezoelectric sensor soldered wire, while the other was not attached to the plate directly. This problem was solved with the help of the magnet of a copper cable. Fig. 3 shows the binding of the probes to the Al 7075 sample. After the probes were attached, measurements of the real part impedance data were performed at room temperature. In these measurements, the frequency range was 2 kHz-80 kHz in 1000 steps.

Figure 3. Attaching probes to the sample (Al 7075)

2.2. Numerical Method

In this section, the behavior of the constrained piezoelectric sensor at varying temperatures was modeled using ANSYS multi-physics software. SOLID5 element was used for PWAS. SOLID45 element was used for aluminum. According to Yang's study [20], the effect of the adhesive layer can be neglected, so this effect was not taken into account.

Material properties of the piezoelectric sensor at room temperature were entered into the ANSYS program using the data published by PI Ceramic, the manufacturer of the sensors supplied for the experimental study, on the internet [23]. The data obtained from the manufacturer cannot be directly entered into the ANSYS program. The necessary conversions should be made to the ANSYS program, as suggested in Imaoka [24]. Using these transformations, the manufacturer's data (25 °C) of the PIC255 piezoelectric sensor were entered into the ANSYS program.

2.2.1. Stiffness / compliance matrix

Elastic compliance (S) is defined as the strain that occurs in the result of the unit stress applied to the piezoelectric material in directions 11 and 33. Also, it can be defined as the inverse of the elastic modulus [25].

$$\left[s^E\right] = \begin{bmatrix} s_{11} & s_{12} & s_{13} & 0 & 0 & 0 \\ s_{12} & s_{11} & s_{13} & 0 & 0 & 0 \\ s_{13} & s_{13} & s_{33} & 0 & 0 & 0 \\ 0 & 0 & 0 & s_{66} & 0 & 0 \\ 0 & 0 & 0 & 0 & s_{44} & 0 \\ 0 & 0 & 0 & 0 & 0 & s_{44} \end{bmatrix}$$

$\left[s^E\right]$ matrix is closely related to the modulus of elasticity, shear modulus and Poisson's ratio (Eqs.1-6).

$$E_X = \frac{1}{s_{11}^E} = E_Y \tag{1}$$

$$E_Z = \frac{1}{s_{33}^E} \tag{2}$$

$$G_{XY} = \frac{1}{s_{66}^E} \tag{3}$$

$$G_{YZ} = \frac{1}{s_{44}^E} = G_{XZ} \tag{4}$$

$$s_{12}^E = NU_{XY}\left(-s_{11}^E\right) \tag{5}$$

$$s_{13}^E = NU_{YZ}\left(-s_{33}^E\right) = NU_{XZ} \tag{6}$$

s_{66}^E and s_{44}^E values are not available in the manufacturer's data. These values are calculated using Eqs. 7- 8.

$$s_{66}^E = 2\left(s_{11}^E - s_{12}^E\right) \quad (7)$$

$$s_{44}^E = 2\left(s_{33}^E - s_{13}^E\right) \quad (8)$$

In literature, there is no function or graphics related to the temperature change of these values of the PIC255 piezoelectric sensors. Therefore, these values were determined using equations.

The change of the Poisson's ratio with temperature is neglected and is assumed to be independent of the direction ($NU_{XY} = NU_{XZ} = NU_{YZ} = \upsilon =$ 0.34). The relationship between the shear modulus and the elastic modulus is defined in Eqs. 9-10.

$$G_{XY} = \frac{E_X}{\left[2\ (1+\ \upsilon)\right]} \quad (9)$$

$$G_{YZ} = G_{XZ} = \frac{E_Z}{\left[2\ (1+\ \upsilon)\right]} \quad (10)$$

The variation of the elastic modulus with temperature is given in Eq.11 [26].

$$E_p(T) = E_p - \frac{(T_0 - T)}{160}\frac{E_P}{4} \quad (11)$$

E_p is Young's modulus at the reference temperature, $E_p(T)$ is Young's modulus at the measured temperature, T is the ambient temperature, T_0 is the reference temperature, p represents the piezoelectricity. The reference temperature is 25 °C. Elastic modules at the reference temperature were calculated using the values of s_{11}^E and s_{33}^E supplied by the manufacturer for the PIC255 piezoelectric sensor. Using Eq.11, the elastic modulus of the PIC255 piezoelectric sensor at temperatures ranging from 0 °C to -45 °C at 5 °C intervals were calculated.

Once the modulus of elasticity has been determined, the shear modulus is calculated for varying temperatures using Eqs. 9 and 10. The shear modules are calculated for the varying temperatures. Using Eqs.1 -8, all the parameters in the $\left[s^E\right]$ matrix were determined for varying temperatures. This data will then be used to determine the conductivity matrix to be calculated and the piezoelectric matrix $[e]$ related to the stress / electric field.

2.2.2. Piezoelectric charge constants

Piezoelectric materials are identified by three piezoelectric charge constants as d_{31}, d_{33} and d_{15} The matrix $[d]$ was created by taking the parameters d_{31}, d_{33} and d_{15} from the catalog values of the manufacturer's.

$$[d] = \begin{bmatrix} 0 & 0 & d_{31} \\ 0 & 0 & d_{31} \\ 0 & 0 & d_{33} \\ 0 & 0 & 0 \\ 0 & d_{15} & 0 \\ d_{15} & 0 & 0 \end{bmatrix}$$

In the ANSYS program, the matrix $[e]$ is the matrix that relates the mechanical stress to the electric field. Using Eq.12, the manufacturer's data has been made available for the ANSYS program.

$$[e] = \left[s^E\right]^{-1}[d] \quad (12)$$

Using the recalculated $\left[s^E\right]^{-1}$ matrices at different temperatures, the $[e]$ matrices were calculated for varying temperatures. The matrix $[d]$ was defined identically for all temperatures and is shown below.

$$[d] = \begin{bmatrix} 0 & 0 & -180 \\ 0 & 0 & -180 \\ 0 & 0 & 400 \\ 0 & 0 & 0 \\ 0 & 550 & 0 \\ 550 & 0 & 0 \end{bmatrix}$$

The $[e]$ matrix generated for 25 ° C is given below.

$$[e] = \begin{bmatrix} 0 & 0 & -7.53378 \\ 0 & 0 & -7.53378 \\ 0 & 0 & 14.19998 \\ 0 & 0 & 0 \\ 0 & 9.912232 & 0 \\ 9.912232 & 0 & 0 \end{bmatrix}$$

2.2.3. Dielectric constants

The relative dielectric constant is the ratio of the amount of load the piezoelectric element can store to the amount of load stored in the vacuum (ε_0 = 8.85x10^{-12} F/m) [27]. The manufacturer data for piezoelectric materials are $\varepsilon_{11} / \varepsilon_0$ and $\varepsilon_{33} / \varepsilon_0$. The temperature-dependent function of the relative dielectric constants is derived from the plot of these values changed with temperature. Fig. 4 shows the percentage change of relative dielectric constants with respect to temperature.

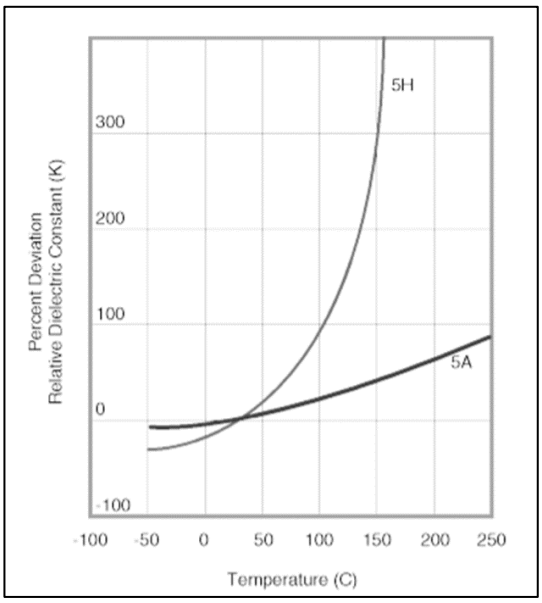

Figure 4. Change of relative dielectric constants according to the temperature [28]

The functions of the relative dielectric constants derived from the temperature dependence were given in Eqs.13-14.

$$\varepsilon_{11}/\varepsilon_0 = 0.0103T^2 + 3.4885T + 1585.4 \quad (13)$$

$$\varepsilon_{33}/\varepsilon_0 = 0.011T^2 + 3.6999T + 1681.5 \quad (14)$$

The coefficient of determination value (r^2) in the two derived equations is 0.99. In these equations, T represents temperature. The values of $\varepsilon_{11}/\varepsilon_0$ and $\varepsilon_{33}/\varepsilon_0$ are calculated for the varying temperatures.

The parameters of $\varepsilon_{11}/\varepsilon_0$ and $\varepsilon_{33}/\varepsilon_0$ cannot be entered directly into the ANSYS program from the manufacturer's catalog values. The manufacturer's data was defined by the matrix $\left[\varepsilon^T\right]$.

$$\left[\varepsilon^T\right] = \begin{bmatrix} \varepsilon_{11}/\varepsilon_0 & 0 & 0 \\ 0 & \varepsilon_{11}/\varepsilon_0 & 0 \\ 0 & 0 & \varepsilon_{33}/\varepsilon_0 \end{bmatrix}$$

Eq. 15 has been used to adapt the manufacturer's data to the ANSYS program.

$$\left[\varepsilon^S\right] = \left[\varepsilon^T\right] - [d]^t \left[s^E\right]^{-1} [d] \quad (15)$$

The $\left[\varepsilon^S\right]$ matrix generated for 25 °C is shown below.

$$\left[\varepsilon^S\right] = \begin{bmatrix} 1033.986 & 0 & 0 \\ 0 & 1033.986 & 0 \\ 0 & 0 & 801.7345 \end{bmatrix}$$

After recalculating $\left[s^E\right]^{-1}$ and $\left[\varepsilon^T\right]$ matrices for different temperatures, $\left[\varepsilon^S\right]$ matrices were created for varying temperatures using Eq. 15.

2.2.4. Density

The equation proposed in Jyoti's study [26] was used to calculate the change in density at varying temperatures (Eq. 16).

$$\rho = \frac{\rho_0}{\left[\left(1+\alpha\Delta T\right)^3\right]} \quad (16)$$

α (Coefficient of thermal expansion) of the piezoelectric sensor has a value ranging from 4×10^{-6} (1/K) to 8×10^{-6} (1/K) for the manufacturer. Since α is defined as the average thermal expansion coefficient in Eq. 16, α value is assumed to be 6×10^{-6} (1/K). The calculated density values are entered into the ANSYS program without any conversion while developing models for varying temperatures.

2.2.5. The elasticity modulus of samples with piezoelectric sensors added at varying temperatures

Eq. 17 is used for the change of the elasticity module with temperature [29].

$$E(T) = E_0 + \frac{\partial E}{\partial T}(T - T_0) = E_0 + \beta(T - T_0) \quad (17)$$

E_0 is Young's modulus at the reference temperature, E is Young's modulus at the measured temperature, T is the ambient temperature, T_0 is the reference temperature, and β represents the linear change of the Young module with temperature. The temperature-dependent function of the elastic modulus is given in Eq.18.

$$E(T) = \left(-4x10^{-5}\right)T^2 - 0.0398T + 69.936 \quad (18)$$

T represents the ambient temperature in °C, and $E(T)$ represents the elasticity modulus at T temperature in GPa. After this function is substituted in Eq.17, the elastic modulus is calculated.

2.2.6. Damping ratio

In this study, the damping ratio was determined by using viscous damping principles. In viscous damping, the mass product factor value is 0, the β (stiffness product factor) value is greater than 0, and the constant damping ratio value is 0 [30]. Stiffness product factor value is calculated using Naillon equations. In Eqs.19-20, the suggested equations are given [31]

$$\beta = \frac{1}{\omega Q_m} \quad (19)$$

$$\omega = 2\pi f \quad (20)$$

ω is the angular velocity in the largest mode (Hz) and Q_m is the mechanical quality factor. The Q_m value is given as 80 in the PIC 255 piezoelectric sensor manufacturer's data. ω value was determined as the result of an experimental study at 25 °C.

2.2.7. Effective frequency shift (EFS)

Effective frequency shift (EFS) is a simple method to compensate for the effect of temperature and can be applied in a wide variety of configurations under various conditions. By comparing the impedance obtained according to the temperature change with the reference impedance, the frequency shift is performed by forming the loop until the minimum correlation coefficient deviation metric (CCDM) index is obtained. In the calculations, the curves are shifted to the left (until the maximum cross-correlation is obtained) to compensate for this, as the fall of the temperature causes the impedance graphs to shift to the right. The equation of effective frequency shift is given in Eq.21.

$$Re\left(Z_{corr,i}\right) = Re\left(Z_{2,i\pm\Delta f}\right) + \Delta_v \quad (21)$$

$Re\left(Z_{corr,i}\right)$ represents the real part of the corrected real impedance value, $Re\left(Z_{2,i\pm\Delta f}\right)$ i ± Δf is the real impedance value measurement (shifted by Δf), Δ_v represents the average of the difference of the real impedance values between the two signals.

While eight different temperature levels were used in the experimental study, ten different temperature levels were used in the numerical study. RMSD, MAPD (mean absolute percentage deviation) and CCDM were used as damage metrics. EFS algorithm was applied, and temperature compensation was performed according to the CCDM metric.

3. EXPERIMENTAL AND NUMERICAL RESULTS

In this section, the effect of temperature on the constrained piezoelectric sensor was investigated by using experimental and finite element methods. The temperature effect was compensated for by using a compensation algorithm.

3.1. Experimental Results

Impedance measurements of the Al 7075 sample were performed at different temperatures. Measurements taken at room temperature as reference and measurements carried out for other temperatures were compared according to this reference measurement.

Fig. 5 shows the impedance measurement results of Al 7075 at room temperature. In Fig.5, it is clear that the mode amplitude at 26828 Hz is larger than the mode amplitude at 57045 Hz. Thus, experiments focused on the first mode. It was performed in 1000 steps in the frequency range of 20 kHz-30 kHz. Fig. 6 shows the results obtained from experimental studies at different temperatures. Compared to room temperature measurements, the frequency shifts to the right and the amplitude increases as the temperature drops.

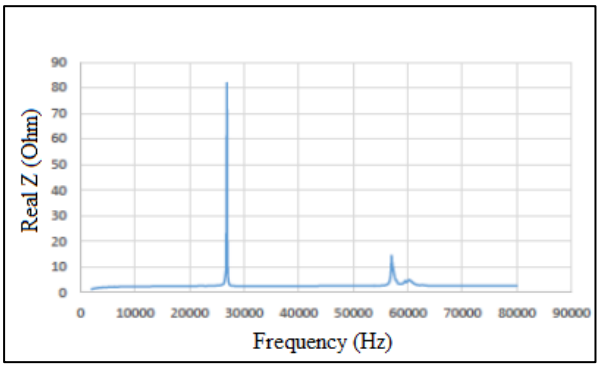

Figure 5. Impedance measurements of Al 7075 sample at 25 °C (Experimental)

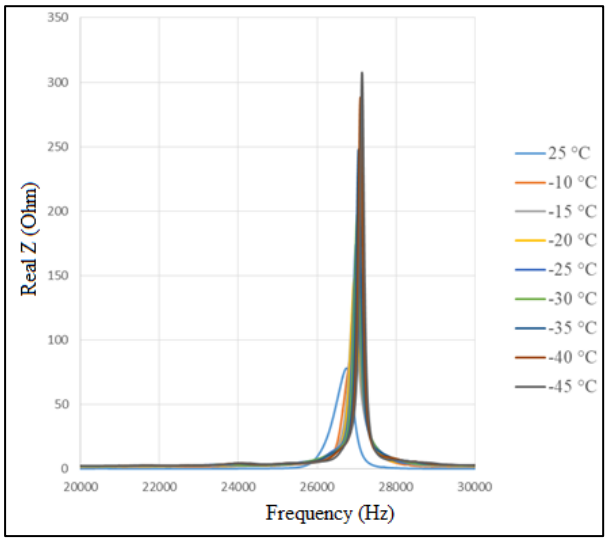

Figure 6. Impedance measurements of Al 7075 sample at varying temperatures (Experimental)

3.2. Numerical Results

The material properties of the piezoelectric sensor and Al 7075 were defined in the ANSYS program. For the damping rate, the mass product factor value was 0, the constant damping ratio was 0, and for β value, Eqs. 19 and 20 were used. The frequency value in the largest mode was set at 26746 Hz in the experimental run at 25 °C. After substituting this value in the Eq. 20, the β value was determined as 7.44×10^{-8} using Eq.19.

The applied voltage value is 0 and 0.5 V, respectively. The number of steps is chosen as 1000, and the frequency range is chosen as 2 kHz-80 kHz, and results are obtained as seen in Fig. 7.

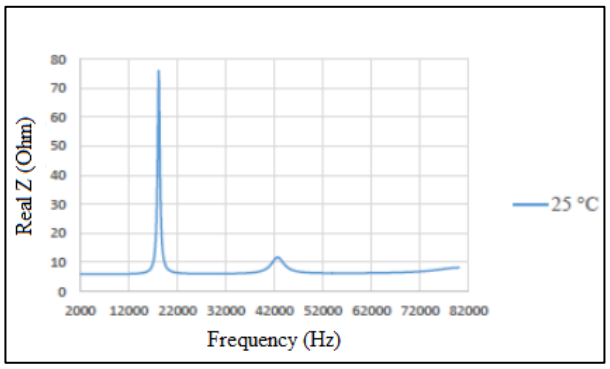

Figure 7. Impedance values of the Al-7075 sample at 25°C (Numerical)

Simulation studies for 25 °C and other temperatures were carried out 15 kHz -25 kHz frequency range as the first mode amplitude larger than the second mode (Fig. 7). For 25 °C, solutions for different mesh numbers were repeated, and the appropriate cell structure was determined by comparison with experimental measurements at 25 °C. The behavior of Al 7075 was examined at temperatures ranging from 0 °C to -45 °C at 5 °C intervals after the appropriate mesh number was determined.

The simulation studies were compared with experimental results using 1625, 5500, 11625 meh numbers. The optimal mesh number was 5500 (4500x1000) chosen at 25 °C when considering the optimum solution time according to different trial simulation studies. 4500 (30x30x5) represents the number of mesh on the plate, and 1000 (10x10x10) represents the number of mesh on the sensor. The selected mesh structure of the specimen was given in Fig.8.

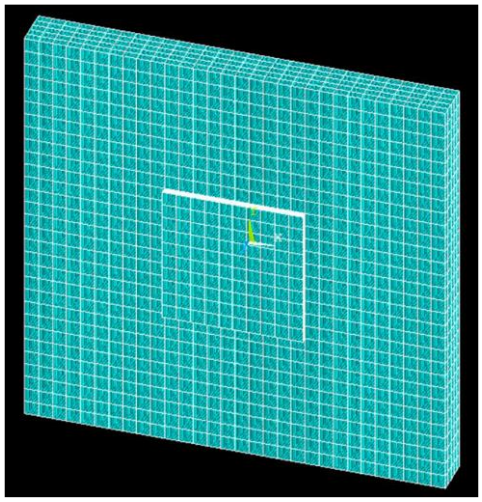

Figure 8. The mesh structure of Al 7075 with a piezoelectric sensor

The simulation results for temperatures ranging from 0 °C to -45 °C at 5 °C intervals using the 4500x1000 cell structure were shown in Fig.9. As seen in the Figure, as the temperature decreases, the frequency shifts to the right and the amplitude value also increases.

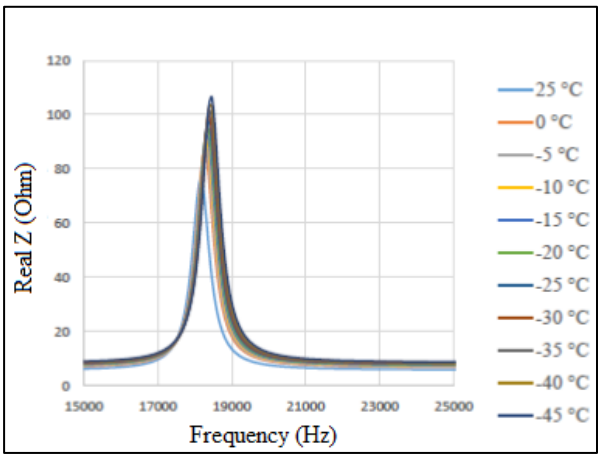

Figure 9. Impedance values of the Al-7075 sample at varying temperatures (Numerical)

3.3. Experimental / Numerical Results in terms of Damage Metrics (non-compensated and compensated)

Non-compensated experimental results by two damage metrics were given in Figs. 10-11. When the results are examined, it is seen that the damage metrics increase as the temperature difference increases. RMSD values range from 0.5 to 2. MAPD values are between 6-11.

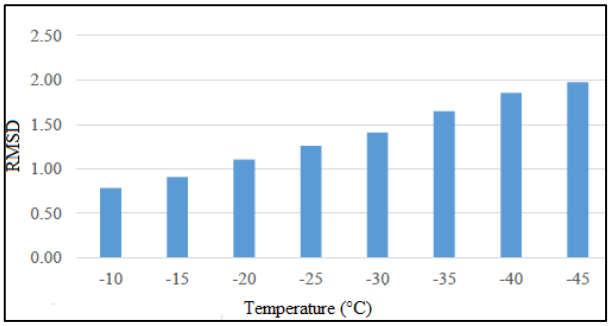

Figure 10. RMSD damage metric values of experimental results at different temperature values (non-compensated)

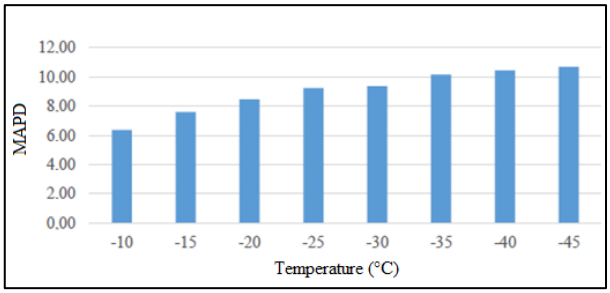

Figure 11. MAPD damage metric values of experimental results at different temperatures (non-compensated)

CCDM metrics before and after compensation were given in Fig.12. These metrics decrease significantly after compensation.

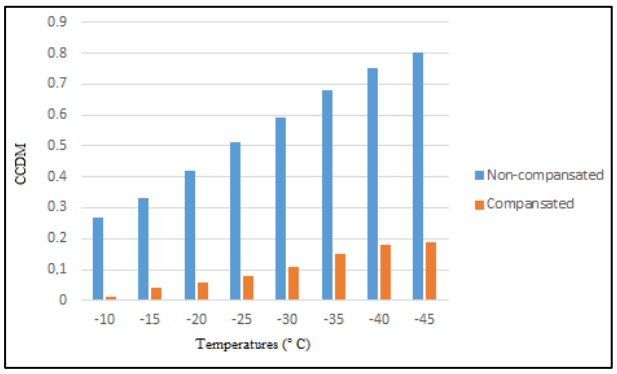

Figure 12. CCDM metrics before and after compensation with hybridized EFS/Genetic algorithm (Experimental)

Compensated experimental results were shown in Figs. 13-14, according to two damage metrics. RMSD values are between 0.25- 1.5. MAPD values range from 6 to 10. After the experimental results have been compensated, the damage metrics have decreased.

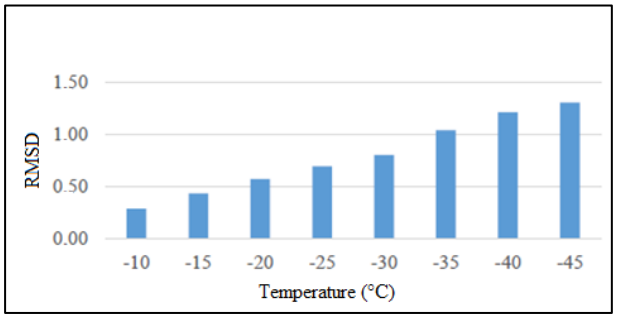

Figure 13. RMSD damage metric values of experimental results at different temperatures(compensated)

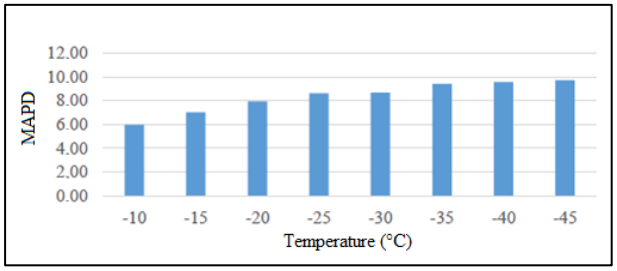

Figure 14. MAPD damage metric values of experimental results at different temperatures (compensated)

Numerical results of non-compensated three damage metrics were given in Figs. 15-16. When the results are examined, the damage metrics increase as the temperature difference increases.

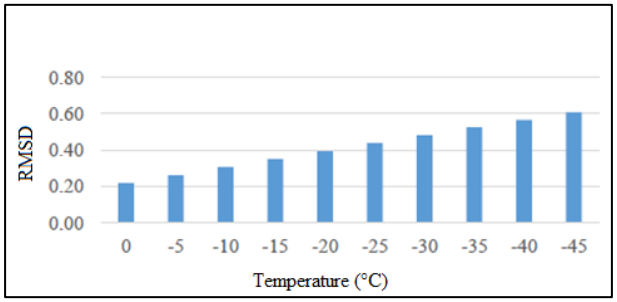

Figure 15. RMSD damage metric values of simulation results at different temperatures (non-compensated)

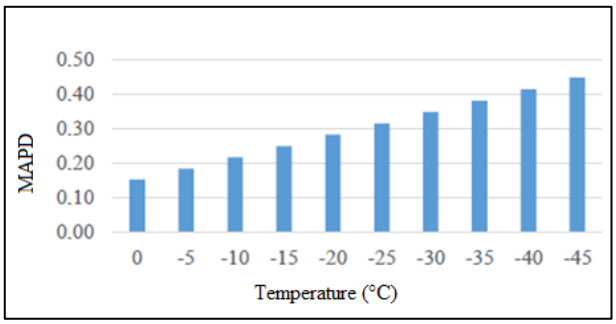

Figure 16. MAPD damage metric values of simulation results at different temperatures (non-compensated)

CCDM metrics before and after compensation were given in Fig.17. These metrics decrease significantly after compensation.

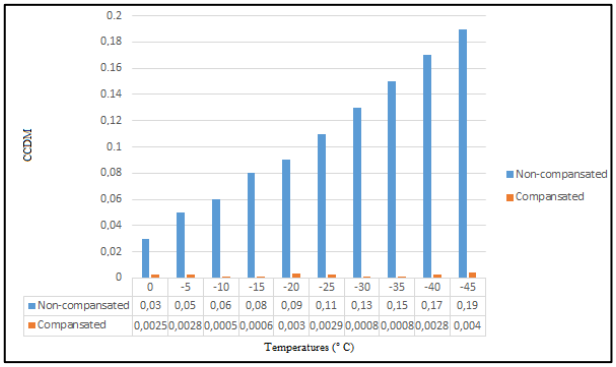

Figure 17. CCDM metrics before and after compensationwith hybridized EFS/Genetic algorithm (simulation)

The numerical results were shown in Figs. 18-19 with two damage metrics. Compensated damage metrics show a decline compared to the non-compensated damage metric values.

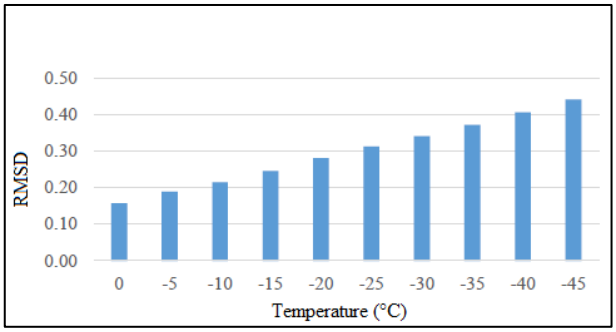

Figure 18. RMSD damage metric values of simulation results at different temperatures (compensated)

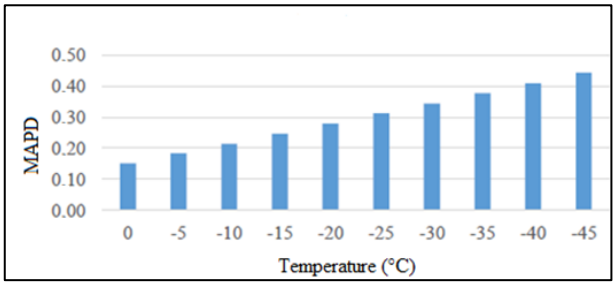

Figure 19. MAPD damage metric values of simulation results at different temperatures (compensated)

In Figs. 20-21, experimental and simulated compensated impedance graphs are given, respectively. Compared to the figures before, the graphs shift to the left.

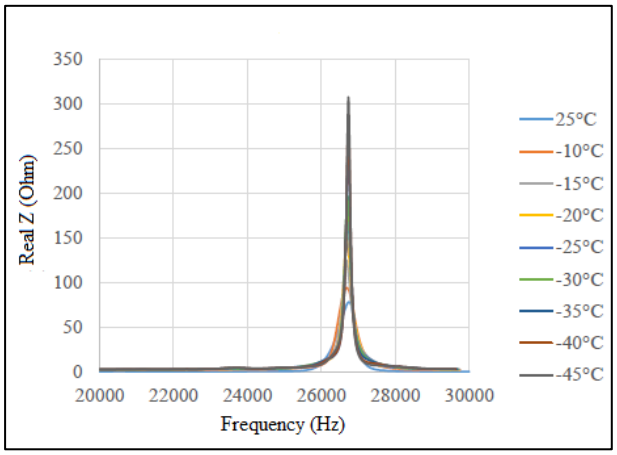

Figure 20. Impedance graphs compensated at different temperatures in the 20-30 kHz frequency band (Experimental)

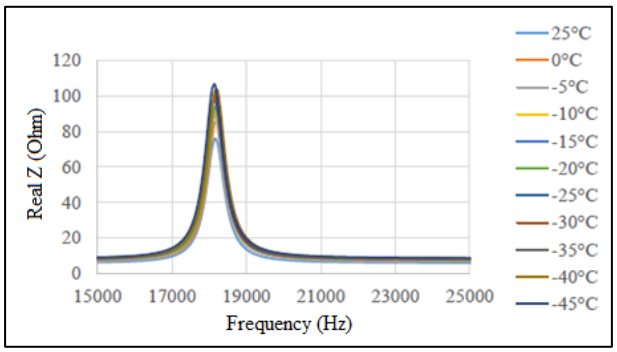

Figure 21. Impedance graph compensated at different temperatures in the 15-25 kHz frequencyband (simulation)

Since the linear variation coefficient of the elasticity module is not defined in the literature for Al 7075, the function of the temperature is taken into consideration after the function is derived from the graph. Therefore, there are differences between experimental and numerical studies.

When all the results are analyzed, the real impedance graphs shift to the right with the temperature decrease. As the temperature change increases, the frequency shift increases. These graphics have been compensated by shifting them to the left. The values of damage metrics have decreased since they were compensated. In this context, it has been found that the results are consistent with the literature studies [6,10,15-17].

4. CURVE/PROBABILISTIC FITTING of DAMAGE METRICS

At this stage of the study, curve / probabilistic fitting was performed using experimentally obtained error metrics. In the first step, curve fitting was applied for the damage metric data that was not compensated. The independent variable was selected as temperature and the RMSD, MAPD and CCDM metrics were used as dependent variables. CURVEEXPERT software was used in the analysis. The results are given in Tables 1-2. The best curves for RMSD, MAPD, and CCDM were Richards, Exponential Association 3, and Sinusoidal curves, respectively.

Since the data is expected to be temperature independent after compensation, the probabilistic fitting has been performed for this data. EASYFIT software was used in the analysis. Kolmogorov-Smirnov and Anderson-Darling tested 56 different distributions by means of the

Table 1. Curve fitting for error metrics

Curves of RMSD	R^2/std.error	Curves of MAPD	R^2/std.error	Curves of CCDM	R^2/std.error
1.Richards	**0.9982/2.38e-2**	**1.Exponential Association 3**	**0.99/1.51e-1**	**1.Sinusoidal**	**0.999/4.8e-3**
2.Reciprocal Quadric	0.9981/2.40e-2	2.Rational model	0.99/1.57e-1	2.Gaussian	0.994/5.47e-3
3.Rational model	0.9982/2.45e-2	3.Heat capacity	0.99/1.68e-1	3.Rational model	0.995/5.4e-3
4.Ratkowsky model	0.9975/2.53e-2	4.Ratkowsky model	0.99/1.72e-1	4.Richards	0.995/5.33e-3

Table 2. Parameters for the best curves

Curves	**Curve equation**	**Parameters**
Richards	$y=a(1+e^{b-cx})^{1/d}$	a=2.1 b=9.5 c=-2.25e-1 d=7.43
Exponential Association 3	$y=a(b-e^{-cx})$	a=8.48 b=1.37 c=-4.9e-2
Sinusoidal	y=a+bcos(cx+d)	a=5.14e-1 b=3.2e-1 c=5.66e-2 d=-3.27

tests for distribution. The results are given in Table 3. In addition, the results of the distribution suitability tests are given in Appendices 1-3. Johnson SB distribution for RMSD, MAPD and Error distribution for CCDM were the most appropriate distributions. In Figure 23, Johnson SB probabilistic distribution for RMSD is shown. The Johnson SB equations are given below (Eqs. 22-23).

$$f(x) = \frac{\delta}{\lambda\sqrt{2\pi z(1-z)}} \exp\left(-\frac{1}{2}(\gamma + \delta \ln\left(\frac{z}{1-z}\right))^2\right) \quad (22)$$

$$z = \frac{x-\zeta}{\lambda} \quad (23)$$

The Error function equations are given below (Eqs. 24-27).

$$f(x) = c_1\sigma^{-1}\exp\left(-|c_o z|^k\right) \quad (24)$$

$$z = \frac{x-\mu}{\sigma} \quad (25)$$

$$c_0 = \left(\frac{\Gamma\left(\frac{3}{k}\right)}{\Gamma\left(\frac{1}{k}\right)}\right)^{1/2} \quad (26)$$

$$c_1 = \frac{kc_0}{2\Gamma\left(\frac{1}{k}\right)} \quad (27)$$

decreased significantly after compensation. Therefore, it has been determined that there are no defects in the structure. The best curves for RMSD, MAPD and CCDM were Richards, Exponential Association 3, and Sinusoidal curves, respectively for non-compensated results. Johnson SB distribution for RMSD, MAPD and Error distribution for CCDM were the most appropriate distributions for experimental compensated damage metrics.

Experimental and simulation results are close to each other. Simulation studies are also considered to be sufficient when there is no possibility of experimental work. In later work, studies can be performed by selecting a wider range of temperatures. Experiments and simulations can be repeated for different sizes of specimens so that it can be determined whether or not the size effect is significant. Furthermore, by studying the behavior of defective samples at varying temperatures, two effects can be evaluated together.

Table 3. Probabilistic fitting of damage metrics (The best probabilistic curves)

RMSD	**Parameters**	**MAPD**	**Parameters**	**CCDM**	**Parameters**
1 Johnson SB	γ -continuous shape parameter=0.12 δ -continuous shape parameter=0.5 λ -continuous scale parameter=1.167 ξ -continuous location parameter=0.25	**1.Johnson SB**	γ -continuous shape parameter=-0.961 δ - continuous shape parameter=0.69 λ -continuous scale parameter=5.82 ξ -continuous location parameter=4.18	**1. Error**	k -continuous shape parameter=100 σ -continuous scale parameter=0.06446 μ -continuous location parameter=0.10125

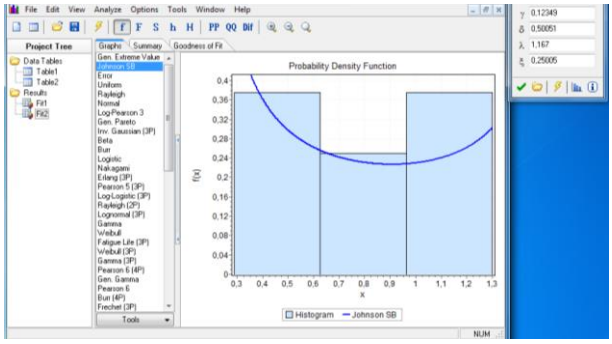

Figure 23. Johnson SB distribution for RMSD

5. CONCLUSIONS

In this study, Al 7075 sample was chosen for the experimental research, considering these structures exposed to varying ambient temperatures. Also, a finite element model considering the temperature effect on the piezoelectric sensor and Al 7075 sample was proposed. The behavior of the constrained piezoelectric sensor/Al7075 for varying temperatures has been investigated. It has been observed that as the temperature decreases, the frequency shifts to the right (increases) and the amplitude increases. This change has been compensated by using EFS Three damage metrics EMI technique has great potential, a lot of work is being done to resolve several problems. Future studies should focus more on real structures to identify critical problems using the EMI technique because most of the researches are conducted under laboratory conditions. Continuous research and advances in computer technologies will bring new solutions and ideas. Also, Artificial neural network approach can be integrated into EMI.

ACKNOWLEDGEMENT

This work was supported by the Scientific Research Projects Commission of Eskişehir Osmangazi University as project number 201715A119.

DECLARATION OF ETHICAL STANDARDS

The author(s) of this article declare that the materials and methods used in this study do not require ethical committee permission and/or legal-special permission.

AUTHORS' CONTRIBUTIONS

Gökhan Haydarlar: Performed the experiments and analysed the results.

Mesut Tekkalmaz: Performed the numerical analysis.

Mehmet Alper Sofuoğlu: Performed the curve/probabilistic fitting of damage metrics and wrote the manuscript.

CONFLICT OF INTEREST

There is no conflict of interest in this study.

REFERENCES

[1] Shankar R.,"***An integrated approach for structural health monitoring***", PhD thesis, Indian Institute of Technology Delhi, Department of Civil Engineering, India, (2009).

[2] Aktan A. E., Helmicki A. J., Hunt V. J., "Issues in health monitoring for intelligent infrastructure", ***Smart Materials and Structures***, 7(5): 674-692, (1998).

[3] Doebling S. W., Farrar C. R., Prime M. B., "A summary review of vibration-based damage identification methods, ***The Shock and Vibration Digest***, 30(2): 91-105, (1998).

[4] Hooker M. W., "***Properties of PZT-based Piezoelectric Ceramics between 150 and 250 °C***", Technical Report, National Aeronautics and Space Administration, (1998).

[5] Grisso B. L., Inman D. J., "Temperature corrected sensor diagnostics for impedance-based SHM", ***Journal of Sound and Vibration***, 329(12): 2323-2336, (2010).

[6] Sepehry N., Shamshirsaz M., Bastani A., "Experimental and theoretical analysis in impedance-based structural health monitoring with varying temperature", ***Structural Health Monitoring: An International Journal,*** 10(6): 573-585, (2010).

[7] Freitas V. F., Santos I. A., Botero É., Fraygola B. M., Garcia D., Eiras J. A., "Piezoelectric Characterization of (0.6)BiFeO3-(0.4)PbTiO3 Multiferroic Ceramics", ***Journal of the American Ceramic Society***, 94(3): 754-758, (2011).

[8] Gupta V., Sharma M., Thakur N., Singh S. P., "Active vibration control of a smart plate using a piezoelectric sensor–actuator pair at elevated temperatures", ***Smart Materials and Structures***, 20(10): 105023:1-13, (2011).

[9] Bukhari S., Islam M., Haziot A., Beamish J., "Shear piezoelectric coefficients of PZT, $LiNbO_3$and PMN-PT at cryogenic temperatures", ***Journal of Physics: Conference Series***, 568(3): 032004:1-5, (2014).

[10] Baptista, F. G., Budoya, D. E., de Almeida, V. A., Ulson, J. A., "An experimental study on the effect of temperature on piezoelectric sensors for impedance-based structural health monitoring", ***Sensors (Basel)***, 14(1): 1208-1227, (2014).

[11] Zou D., Liu T., Liang C., Huang Y., Zhang F., Du C., "An experimental investigation on the health monitoring of concrete structures using piezoelectric transducers at various environmental temperatures", Journal of Intelligent Material Systems and Structures, 26(8):1028-1034, (2015).

[12] Amezquita-Sanchez J., Valtierra-Rodriguez M., Aldwaik M., Adeli H., "Neurocomputing in Civil Infrastructure", ***Scientia Iranica***, 23(6): 2417-2428, (2016).

[13] Fallahian S., Joghataie A., Kazemi M., "Structural damage detection using time domain responses and teaching–learning-based optimization (TLBO) algorithm", ***Scientia Iranica***, (2017) doi: 10.24200/sci.2017.4238

[14] Rabelo D.S., Steffen V., Neto R.M.F. and Lacerda H.B., "Impedance-based structural health monitoring and statistical method for threshold-level determination applied to 2024-T3 aluminum panels under varying temperature", ***Structural Health Monitoring***, 16(4): 365-381, (2017).

[15] Wandowski T., Malinowski P. H., Ostachowicz W. M., "Delamination detection in CFRP panels using EMI method with temperature compensation", ***Composite Structures***, 151: 99-107, (2016).

[16] Xu G., Xu B., Xu C., Luo Y., "Temperature effects in the analysis of electromechanical impedance by using spectral element method", ***Multidiscipline Modeling in Materials and Structures***, 12(1): 119-132, (2016).

[17] Haider M. F., Giurgiutiu V., Lin B., Yu L., "Irreversibility effects in piezoelectric wafer active sensors after exposure to high temperature", ***Smart Materials and Structures***, 26(9): 095019:1-14, (2017).

[18] Rezvani K. Maia M., Sabour M., "Comparison of Some Methods for Structural Damage Detection", ***Scientia Iranica***, 25(3): 1312-1322, (2018).

[19] Tseng K.K., Wang L., "Smart piezoelectric transducers for in situ health monitoring of concrete", ***Smart Materials and Structures.,*** 13(5): 1017-1024, (2004).

[20] Yang Y., Lim Y. Y., Soh C. K., "Practical issues related to the application of the electromechanical impedance technique in the structural health monitoring of civil structures: I. Experiment", ***Smart Materials and Structures***, 17(3): 035008:1-14, (2008).

[21] Lim Y.Y., Soh C.K., "Fatigue life estimation of a 1D aluminum beam under mode-I loading using the electromechanical impedance technique", ***Smart Materials and Structures,*** 20(12): 125001:1-12, (2011).

[22] Hamzeloo S.R., Shamshirsaz M., Rezaei S.M., "Damage detection on hollow cylinders by electro-mechanical impedance method: Experiments and finite element modeling", ***C. R. Méc.***, 340: 668–677, (2012).

[23]***https://www.piceramic.com/en/products/piezoceramic-materials/#c15162,*** "PI Ceramic Piezoelectric Materials-Material Data", (1996).

[24] Imaoka S, ***Ansys tip of the week: Conversion of piezoelectric material data***, (http://ansys.net/ansys/tips/Week13 TNT Conversion of Piezoelectric Material Data. pdf), (1999).

[25] Türker Ö., ***"Designing And Manufacturing of PZT/ Polymer Based Smart Beams Which Compatible Active Vibration Control"***, Master Thesis, Istanbul Technical University, Istanbul, Turkey, (2009).

[26] Jyoti A., "Modelling and analysis of PZT Micro power Generator", ***PhD Thesis***, Auburn University, (2008).

[27] ***http://www.americampiezo.com***, "APC International Ltd. Product Manual- Piezoelectric Ceramic: Principles and Applications", (2006).

[28] ***http://www.piezo.com/catalog8.pdf,*** "Piezo System Inc.", (1997).

[29] Kabeya K. I., "Structural Health Monitoring Using Multiple Piezoelectric Sensors and Actuators", ***Master of Science thesis***, VirginiaTech University, (1998).

[30] Lerch R., 1990, "Simulation of piezoelectric devices by two- and three-dimensional finite elements", ***IEEE Trans Ultrason Ferroelectr Freq Control,*** 37(3): 233-247, (1990).

[31] Naillon M., Coursant R., Besnier F., "Analysis of piezoelectric structures by a finite-element method", ***Acta Electronica***, 25(4): 341-362, (1983).

APPENDICES

A.1.Goodness of Fit - Details/RMSD

Johnson SB [#28]
Kolmogorov-Smirnov
Sample Size=8
Statistic=0.11096
P-Value=0.99969
a
0.2
0.1
0.05
0.02
0.01
Critical Value
0.35831
0.40962
0.45427
0.50654
0.54179
Reject?
No
No
No
No
No
Anderson-Darling
Sample Size=8
Statistic=0.14633
Rank
a
0.2
0.1
0.05
0.02
0.01
Critical Value
1.3749
1.9286
2.5018
3.2892
3.9074
Reject?
No
No
No
No

A.2.Goodness of Fit - Details/MAPD

Johnson SB [#30]
Kolmogorov-Smirnov
Sample Size=8
Statistic=0.14144
P-Value=0.98937
a
0.2
0.1
0.05
0.02
0.01
Critical Value
0.35831
0.40962
0.45427
0.50654
0.54179
Reject?
No
No
No
No
No
Anderson-Darling
Sample Size=8
Statistic=0.17222
a
0.2
0.1
0.05
0.02
0.01
Critical Value
1.3749
1.9286
2.5018
3.2892
3.9074
Reject?
No
No
No
No
No

A.3. Goodness of Fit - Details/CCDM

Error [#9]
Kolmogorov-Smirnov
Sample Size=8
Statistic=0.14725
P-Value=0.98408
a
0.2
0.1
0.05
0.02

0.01	0.1
Critical Value	0.05
0.35831	0.02
0.40962	0.01
0.45427	Critical Value
0.50654	1.3749
0.54179	1.9286
Reject?	2.5018
No	3.2892
No	3.9074
No	Reject?
No	No
No	No
Anderson-Darling	No
Sample Size=8	No
Statistic=0.2047	No
a	
0.2	